Studying the influence of material parameters on quantum efficiency of $In_{0.53}Ga_{0.47}As$ photovoltaic detector

YINGTIAN XU, YING LI[a], BEIHONG LONG[b], YAN MA, GUOTONG DU, JINGZHI YIN[*]
State Key Laboratory on Integrated Optoelectronics, College of Electronic Science and Engineering, Jilin University, 2699 Qianjin Street, Changchun, 130012, People's Republic of China
[a]*Changchun Automobile Industry institute, 9999 Dongfeng street, Changchun, 130011, People's Republic of China*
[b]*College of Materials Science and Engineering, Jinlin University, 2699 Qianjin Street, Changchun, 130012, People's Republic of China*

In this paper, the dependence of quantum efficiency on the direction of incident light, carrier concentrations, surface recombination velocities and material thicknesses for $In_{0.53}Ga_{0.47}As$ photovoltaic detector has been analyzed. When light injected from *p*-side, the *p*-region surface recombination velocity, its carrier concentration and thickness have significant impact to the quantum efficiency. The *n*-region material parameters have slight impact on quantum efficiency. The surface recombination velocity and its thickness influence is primarily for low carrier concentration ($n<10^{17}cm^{-3}$). When light injected from *n*-side, the *n*-region surface recombination velocity affects quantum efficiency when $n<10^{17}cm^{-3}$; the influence of thickness on quantum efficiency is primarily when $n>10^{16}cm^{-3}$.

(Received June 12, 2012; accepted October 30, 2012)

Keywords: $In_{0.53}Ga_{0.47}As$ PV detector, Material parameters, Quantum efficiency

1. Introduction

Due to the prominent features such as relatively low dark current density [1-3], quick response and high sensitivity and detectivity [4 5], Indium Gallium Arsenide ($In_{1-x}Ga_xAs$) ternary alloys have become significant materials for the fabrication of infrared detectors [6 7]. The energy gap of the $In_{1-x}Ga_xAs$ ternary system spans from 0.35 *eV* (3.5μm) for *InAs* to 1.43 *eV* (0.87μm) for *GaAs*. $In_{0.53}Ga_{0.47}As$ alloy (E_g=0.73 *eV*, λ_c=1.7μm) lattice matched to the *InP* substrate has already been shown to be a suitable detector material for near-IR (1.0~1.7μm) spectral range [8 9]. The photovoltiac detectors made by $In_{1-x}Ga_xAs$ have caused much attention in near infrared applications, such as optical fiber communication, spectroscope analysis and remote sensing, infrared imaging and many other fields [10-12].

Detectivity, denoted as *D** is an important parameter to measure detector performance. It is limited by quantum efficiency and zero bias resistance-area product which are determined by material parameters of $In_{1-x}Ga_xAs$ ternary alloys. In this paper, we have analyzed the dependence of quantum efficiency on the direction of incident light, carrier concentrations, surface recomnination velocities and material thickness for $In_{0.53}Ga_{0.47}As$ photovoltaic detector.

2. Theory analysis

The structure of photodetector is the homogenous *p*-*n* type of $In_{1-x}Ga_xAs$ deposited on *InP* substrate at *T*=300*K*. A two-dimensional model of detector is shown in Fig. 1. The light is injected from the *p*-region (a) or *n*-region (b).

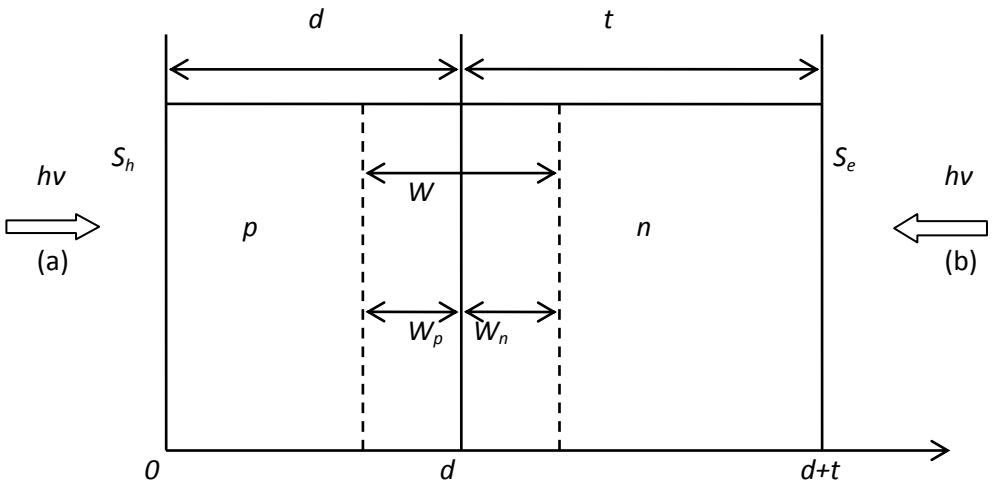

Fig. 1. Schematic 2D structure of $In_{1-x}Ga_xAs$ p-n junction, the light is injected from the p-region (a) or n-region (b).

S_h and S_e are surface recombination velocity (*m/s*) for holes in *n* region and for electrons in *p* region; *t* and *d* are the thickness for *n* and *p*-region thickness (μm); the *n* and *p* are carrier concentration in *n*-region and *p*-region (cm^{-3}); *W* is width of depletion region (μm); W_n is width of depletion region on *n* side (μm); W_p is width of depletion region on *p* side (μm). Usually, characterize the performance of Infrared photovoltaic detector by detectivity *D**, which depends on the zero-bias resistance junction-area product (R_0A) and quantum efficiency (η), the equation of *D** is given by:

$$D^* = \frac{\lambda \eta q}{hc}\sqrt{\frac{R_0 A}{4kT}} \tag{1}$$

where η and *k* are quantum efficiency and Boltzmann constant, *T* is the work temperature, λ is the wavelength of the incidence light, *q* is the charge of an electron and *c* is the velocity of light. In order to get the equation of η, photocurrent equation has to be formulated first. It involves in five basic equations [13]: two current density equations, two continuity equations for electron and hole in *p*-region and *n*-region respectively, and a Poisson's equation. The photocurrent densities in different regions are obtained when the incident light is injected from the *n*-region. They are given by [14],

$$J_{n,ph} = \frac{\alpha q L_h (1-r)\varphi}{(\alpha^2 L_h^{\,2}-1)}\left\{\frac{(r_h+\alpha L_h)-e^{-\alpha(t-W_n)}[r_h \operatorname{ch}(\frac{t-w_n}{L_h})+\operatorname{sh}(\frac{t-w_n}{L_h})]}{r_h \operatorname{sh}(\frac{t-w_n}{L_h})+\operatorname{ch}(\frac{t-w_n}{L_h})}-\alpha L_h e^{-\alpha(t-W_n)}\right\} \tag{2}$$

$$J_{p,ph} = \frac{\alpha q L_e (1-r)\varphi}{(\alpha^2 L_e^{\,2}-1)} e^{-\alpha(t+W_p)}\left\{\alpha L_e+\frac{(r_e-\alpha L_e)e^{-\alpha(d-W_p)}-[r_e \operatorname{ch}(\frac{d-w_p}{L_e})+\operatorname{sh}(\frac{d-w_p}{L_e})]}{r_e \operatorname{sh}(\frac{d-w_p}{L_e})+\operatorname{ch}(\frac{d-w_p}{L_e})}\right\} \tag{3}$$

$$J_{dr,ph} = q\varphi(1-r)[e^{-\alpha(t-W_n)}-e^{-\alpha(t+W_p)}] \tag{4}$$

Where $J_{n,ph}$, $J_{p,ph}$, and $J_{dr,ph}$ are photocurrent densities of *n*-region, *p*-region and depletion region, respectively. α、φ 、 *r* are the absorption coefficient, light flux and reflection coefficient, respectively. $D_i = kT\mu_i / q$, $L_i = (D_i\tau_i)^{1/2}$ and $\gamma_i = L_i S_i / D_i$, the angle mark *i* namely represents *e* or *h*. *L*, *S*, μ, *D* and τ are the diffusion length (*cm*), surface recombination velocity (ms^{-1}), effective mobility ($cm^2V^{-1}s^{-1}$), diffusion coefficient (cm^2s^{-1}), and carrier lifetime (*s*) for holes in the *n* region or for electrons in the *p* region, respectively. n_i is the intrinsic carrier concentration (cm^{-3}). Therefore, the total photocurrent densities J_{ph} is given by:

$$J_{ph} = J_{n,ph} + J_{p,ph} + J_{dr,ph} \tag{5}$$

At the steady-state, the relationship of total photocurrent density J_{ph} and total quantum efficiency η shows as following [15]:

$$J_{ph} = \eta q \varphi \tag{6}$$

The quantum efficiency of *n*-region, *p*-region and depletion region is derived from above equations.

$$\eta_n = \frac{\alpha L_h (1-r)}{(\alpha^2 L_h^{\,2}-1)}\left\{\frac{(r_h+\alpha L_h)-e^{-\alpha(t-W_n)}[r_h \operatorname{ch}(\frac{t-w_n}{L_h})+\operatorname{sh}(\frac{t-w_n}{L_h})]}{r_h \operatorname{sh}(\frac{t-w_n}{L_h})+\operatorname{ch}(\frac{t-w_n}{L_h})}-\alpha L_h e^{-\alpha(t-W_n)}\right\} \tag{7}$$

$$\eta_p = \frac{\alpha L_e (1-r)}{(\alpha^2 L_e^{\,2}-1)} \mathrm{e}^{-\alpha(t+W_p)}\left\{\alpha L_e+\frac{(r_e-\alpha L_e)\mathrm{e}^{-\alpha(d-W_p)}-[r_e \operatorname{ch}(\frac{d-w_p}{L_e})+\operatorname{sh}(\frac{d-w_p}{L_e})]}{r_e \operatorname{sh}(\frac{d-w_p}{L_e})+\operatorname{ch}(\frac{d-w_p}{L_e})}\right\} \tag{8}$$

$$\eta_{dr} = (1-r)[e^{-\alpha(t-W_n)} - e^{-\alpha(t+W_p)}] \quad (9)$$

$$\eta = \eta_n + \eta_p + \eta_{dr} \quad (10)$$

If light is injected from *p*-region, the quantum efficiency of *n*-region, *p*-region, and depletion region are the same as (7)-(10). But corresponding parameter marked should be exchanged, that is $n \to p$, $r_e \to r_h$, $L_e \to L_h$, $W_p \to W_n$, $t \to d$, $p \to n$, $r_h \to r_e$, $L_h \to L_e$, $W_n \to W_p$, $d \to t$.

Material parameters of $In_{0.53}Ga_{0.47}As$ ternary-alloy used in this paper are obtained by the method of linear interpolation. The other related material parameters are listed in Table 1.

Table 1. Material parameters of InAs and GaAs.

Alloy	*Eg(T)(eV)*	ε_r	m_e^*/m_0	m_h^*/m_0	m_s^*/m_0	Δ
InAs	$0.420 - 2.5010^{-4} T^2/(T+75)$	14.5	0.023	0.41	0.089	0.38
GaAs	$1.519 - 5.4010^{-4} T^2/(T+204)$	13.18	0.067	0.45	0.15	0.34

3. Results and analysis

We analyzed the influence of carrier concentrations, thickness, the surface recombination velocities in the two quasi-neutral regions and direction of incident light on quantum efficiency. The calculation is performed on an $In_{0.53}Ga_{0.47}As$ PV detector operated at 300 *K*. In the calculation, the electron and hole mobility are μ_e=5000$cm^2/V \cdot s$ and μ_p=400$cm^2/V \cdot s$, respectively; The wavelength of the incident light is λ=1.4μm.

The wavelength and direction of incident light have a significant influence on the quantum efficiency. Fig. 2 shows that the quantum efficiency depends on the light wavelength and the incidence direction.

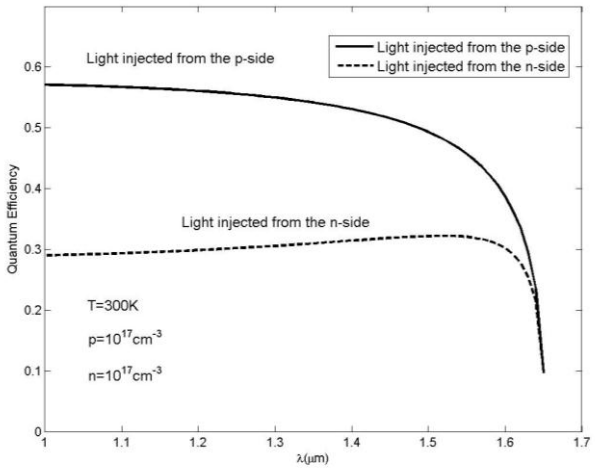

Fig. 2. Relationship between quantum efficiency and direction of incident light with d=2μm, t=2μm, S_e=0, S_h=0, x=0.47.

It indicates that quantum efficiency of light injected from the *p*-side is larger than the one injected from *n*-side at the same parameters. This can be explained that diffusion of minority carrier has impact on quantum efficiency. The electronic diffusion length of the *p*-region is longer than holes' diffusion length of *n*-region, because the mobility of electrons is higher than that of the holes. Therefore, when light is injected from the *p*-side, a larger number of minority carriers which generated by light absorption is arrived at *p*-*n* junction. The number is larger than that produced by light injected from the *n*-side. These carriers contribute to photocurrent, which determine the quantum efficiency.

Firstly, the quantum efficiency of light injected from *p*-side has been analyzed. Fig. 3 distinctly shows that quantum efficiency versus the *p*-region carrier concentration (*p*) with the surface recombination velocity (S_e).

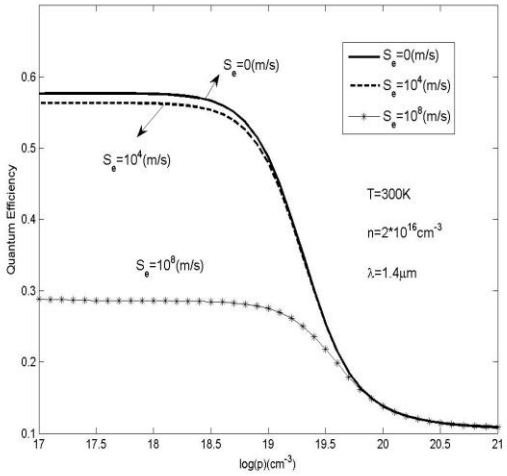

Fig. 3. The quantum efficiency versus the p-side carrier concentration p with the S_e, d=2μm, t=4μm, S_h=0, x=0.47.

Quantum efficiency can be achieved 50~60% when λ=1.4μm and p is at $10^{17}cm^{-3}$~$10^{19}cm^{-3}$, which is consistent with experimental values reported by T. P. Pearsall et al [16, 17] at carrier concentration p=$10^{18}cm^{-3}$, n=10^{16} cm^{-3}. The dependence of quantum efficiency on carrier concentration in the range of p=$10^{17}cm^{-3}$~10^{21} cm^{-3} with different surface recombination velocity has been researched. The result shows that quantum efficiency versus carrier concentration behave differently in three different concentration ranges, low doping concentration ($10^{17}cm^{-3}$~$10^{18}cm^{-3}$), high doping concentration ($10^{20}cm^{-3}$~$10^{21}cm^{-3}$) and intermediate region ($10^{18}cm^{-3}$~$10^{20}cm^{-3}$). Quantum efficiency is almost independent of p at low concentration, but deceased significantly at intermediate region. Such decrease trend slows down at high concentration. High quantum efficiency can be achieved with an optimized doping concentration. Therefore, this result will play a key role to improve detector performance. In addition, the figure indicates that quantum efficiency reduces with the increasing of surface recombination velocity at the range of p=$10^{17}cm^{-3}$~10^{19} cm^{-3} and the quantum efficiency rapid reduces within p>10^{19} cm^{-3} for S_e≤$10^4m/s$. It means that surface recombination velocity has great influence on quantum efficiency. Passivation is one of methods to decrease surface recombination velocity, in order to obtain high quantum efficiency.

The effect of p-region carrier concentration (p) and thickness (d) on quantum efficiency is presented by Fig. 4. When p=$10^{17}cm^{-3}$ and d=10μm, relatively higher quantum efficiency will be obtained (η>60%) in Fig. 4(a). Moreover, quantum efficiency increases with thickness of p-region in the $log_{10}(p)$<17.8. When p-region is heavily doped about p^+=$10^{19}cm^{-3}$~$10^{20}cm^{-3}$, quantum efficiency for the 0.7μm p-region thickness is larger than the one for 1.2μm p-region thickness. This conclusion has been confirmed in the literature of Nobuhiko Susa et al [18]. It is difficult to analyze the relationship of quantum efficiency versus p-region thickness and carrier concentration directly; Fig. 4(b) provides the dependence of η on d with p-region carrier concentration as a parameter. When p=$10^{19}cm^{-3}$, the η appears a peak about 57.68% at d=0.7μm, and η tends to decrease with increasing of d. For p=$10^{17}cm^{-3}$ and p=$10^{18}cm^{-3}$, η gradually increases from d<3μm and reaches to about 60% at d=3μm. Furthermore, increasing p-region thickness from 3μm to 10μm, quantum efficiency have a slight decline for p=$10^{18}cm^{-3}$, and almost unchanged for p=$10^{17}cm^{-3}$. It indicates that p-region carrier concentration at $10^{17}cm^{-3}$~$10^{18}cm^{-3}$ will improve quantum efficiency, which coincides with that in Fig. 3. Meanwhile, the p-region thickness needs to be adjusted to obtain high quantum efficiency.

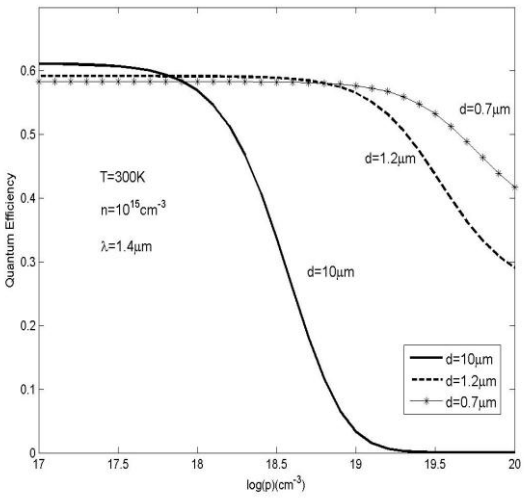

(a)

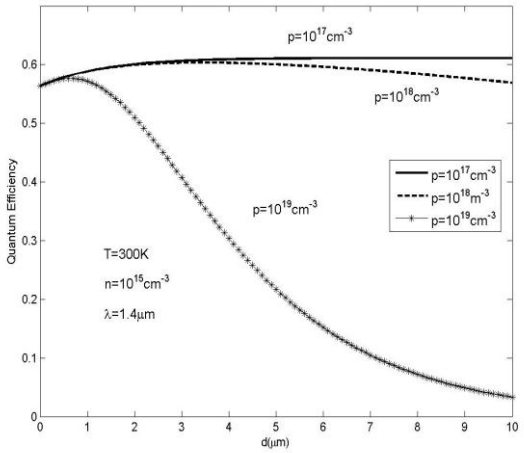

(b)

Fig. 4. (a) The quantum efficiency versus the p-region carrier concentration with thickness of p-region. (b) The quantum efficiency versus the thickness of p-region with p- region carrier concentration. t=3.5 μm, S_h=0, S_e=0, x=0.47.

Fig. 5 provides the dependence of quantum efficiency on p-region thickness (d) with different p-side surface recombination velocity (S_e). At the initial stage, quantum efficiency is increasing with d, and arrives at largest value for different S_e. Subsequently, quantum efficiency tends to be saturated for S_e=0, but quantum efficiency reduces for other S_e. The high quantum efficiency is obtained for S_e=0 within d≥5μm, which is about 60%. The high quantum efficiency can only be achieved in a certain p-region thickness for $S_e \neq 0$.The largest η is got about 55% at d=5μm for S_e=$10^4m/s$ and about 20% at d=2μm for S_e=$10^8m/s$.

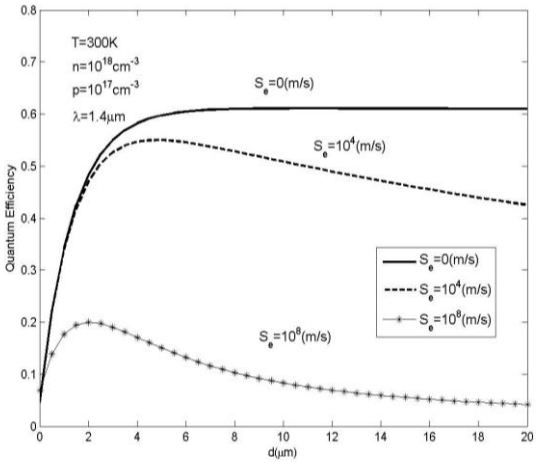

Fig. 5. The quantum efficiency versus the thickness of p-region with different p - side surface recombination velocity at t=5μm, S_h=0, x=0.47.

The relationship between the quantum efficiency and *n*-region parameters has been provided in Fig. 6 at $p=10^{17}cm^{-3}$. The change of the quantum efficiency (η) with carrier concentration in *n*-region (*n*) as a function of *n*-side surface recombination velocity (S_h) has been shown in Fig. 6 (a). The quantum efficiency versus carrier concentration in *n*-region with different *n*-region thickness (*t*) has been provided in Fig. 6 (b). In Fig. 6 (a), the quantum efficiency declines about 2.37% with the increase of carrier concentration in *n*-region from $n=10^{15}cm^{-3}$ to $n=10^{19}cm^{-3}$ at S_h=0(*m/s*), and η decreases less than 2.37% at $S_h\neq0$ (*m/s*). The same trend has been shown in Fig. 6 (b) that η decreases slightly with *n* increasing from $n=10^{15}cm^{-3}$ to $n=10^{19}cm^{-3}$ at different width of *n*-region. It can be explained that the light is mainly absorbed in *p*-region, which lead the light intensity to be attenuated when light arrived at *n*-region. Therefore, the light absorption is reduced in *n*-region. It reflected that *n*-side surface recombination velocity and *n*-region thickness has fewer impacted on quantum efficiency. In addition, the effect of S_h and *t* on quantum efficiency is mainly in low carrier concentration of *n*-region. At range of high carrier concentration of *n*-region, the same quantum efficiency has been achieved independent of S_h or *t*.

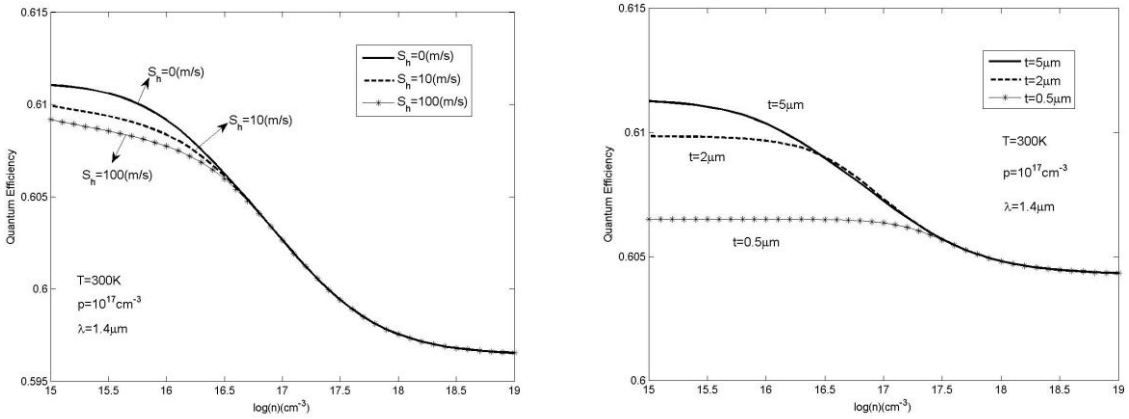

(a) (b)

Fig. 6. (a) The quantum efficiency versus carrier concentration in n-region with n-side surface recombination velocity at t=5μm. (b) The quantum efficiency versus carrier concentration in n-region with the thickness of n-region at S_h=0. d=5μm,S_e=0, x=0.47.

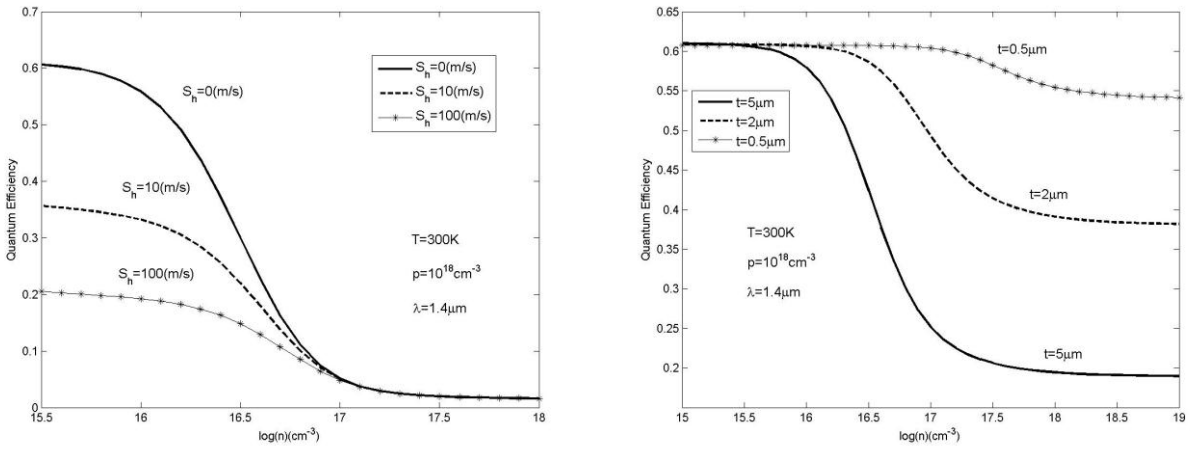

(a) (b)

Fig. 7. (a) The relationship between quantum efficiency and n-region carrier concentration for different S_h at t=5μm. (b) The dependence of quantum efficiency on n-region carrier concentration with the thickness t as a parameter at S_h=0. d=5μm, S_e=0, x=0.47.

Furthermore, we have studied the dependence of quantum efficiency on material parameters when incident light is injected from the *n*-region in Fig. 7. The relationship between quantum efficiency and the *n*-region carrier concentration for different S_h is showed in Fig. 7 (a). It shows that the effect of surface recombination velocity on quantum efficiency is primarily in $n<10^{17}cm^{-3}$ and the quantum efficiency will be improved with the decrease of surface recombination velocity in *n*-region. When carrier concentration in *n*-region increases from $n=10^{16}cm^{-3}$ to $n=10^{17}cm^{-3}$, the quantum efficiency has a stepwise decreases independent of S_h value. It can be explained that with increase of *n*-region carrier concentration, the diffusion length of *n*-region minority carrier is reduced, these minority carriers recombined before they arrived at *p*-*n* junction, thereby, quantum efficiency is dropped. In addition, the increase of *n*-side surface recombination velocity leads to increase of the recombination of photo-generated minority carriers on surface. Therefore, the decrease of quantum efficiency is due to the reducing number of minority carriers which arrived at *p*-*n* junction. Fig. 7 (b) shows the quantum efficiency versus *n*-region carrier concentration with the thickness (*t*) as a parameter. It shows that the quantum efficiency rapidly declines with increasing of *t* in $n>10^{16}cm^{-3}$. This can be attributed to that the diffusion length of *n*-region minority carrier becomes shorter with the *n*-region thickness increasing, therefore, the recombination of photo-generated carriers is increase, and consequently quantum efficiency is reduced.

4. Conclusion

In this paper, we analyzed the effect of carrier concentrations, thickness, surface recombination velocities in the two quasi-neutral regions and the direction of incident light on quantum efficiency. When light is injected from *p*-side, *p*-region surface recombination velocity, *p*-region carrier concentration and *p*-region thickness have significant influence on quantum efficiency. It concluded that high quantum efficiency (η>60%) can be achieved, if *p*-region thickness is about $10\mu m$ for low carrier concentration ($p=10^{17}cm^{-3}$). Furthermore, when *p*-region carrier concentration is about $p=10^{19}\mathrm{cm}^{-3}$, quantum efficiency reaches to a peak value about η=57.68% when the region thickness is about $d=0.7\mu\mathrm{m}$. The material parameters of *n*-region have less effect on quantum efficiency. The influence of S_h and *t* on quantum efficiency is mainly at low carrier concentration of *n*-region ($n<10^{17}cm^{-3}$). When light is injected from *n*-side, the *n*-region surface recombination velocity affects quantum efficiency mainly at $n<10^{17}cm^{-3}$; the influence of thickness on quantum efficiency is mostly at $n>10^{16}cm^{-3}$. These results will provide benefit for designing and fabrication of the *InGaAs* PV detectors.

Acknowledgements

This work was supported by Natural Science Foundation of China Contract No. 60676039, 863 Project of China Contract No. 2007AA06Z112, the Science and Technology Department of Jilin Province under Grant No 20070709.

Reference

[1] Xiaofeng Duan, Yongqing Huang, Xiaomin Ren, Yufeng Shang, Xinye Fan, Fuquan Hu. IEEE Photonics Technology Letters. **24**(10), 863 (2012).
[2] Liu Shao-Qing, Han Qin, Zhu Bin, Yang Xiao-Hong, Ni Hai-Qiao, Hf Ji-Fang, Wang Xin, Niu Zhi-Chuan. Chin. Phys. Lett. **29**(3), 038501 (2012).
[3] Michael MacDougal, Jon Geske, Chad Wang, David Follman. Optical Engineering. **50**(6), 061011 (2011).
[4] A. Tosi, F. Acerbi, A. Dalla Mora, M. A. Itzler, X. Jiang. IEEE Photonics Journal. **3**(1), 31 (2011).
[5] J. Kaniewski, J. Piotrowski. Opto-Electronics Review. **12**(1), 139 (2004).
[6] Cheng Li, Yonggang Zhang, Kai Wang, Yi Gu, Haosibaiyin Li, YaoYao Li. Infrared Physics & Technology. **53**, 173 (2010).
[7] S. Ozer, O. O. Cellek, C. Besikci. Infrared Physics & Technology. **47**, 115 (2005).
[8] A. Rogalski. Progress in Quantum Electronics. **27**, 59 (2003).
[9] Lars Zimmermann, Joachim John, Stefan Degroote, Gustaaf Borghs, Chris Van Hoof. Appl. Phys. Lett. **82**, 2838 (2003).
[10] Henry Yuan, Jongwoo Kim, Gary Apgar etal. Proc. of SPIE. **6950**, 695000 (2008).
[11] L. Becker. Proc. of SPIE. **5881**, 588105 (2005).
[12] Antoni Rogalski. Infrared Physics & Technology. **43**, 187 (2002).
[13] Y. Tian, Z. Tianming, Z. Baolin, J. Hong, J. Yixin. Solid-state Electronics. **43**, 625 (1999).
[14] R. K. Willardson, A. C. Beer, Semiconductors and Semimetals, Academic Press, United States, **11**, 16 (1975).
[15] R. K. Willardson, A. C. Beer, Semiconductors and Semimetals, Academic Press, United States, **18**, 201 (1981).
[16] T. P. Pearsall, M. Papuchon. Appl. Phys. Lett. **33**, 640 (1978).
[17] T. P. Pearsall. IEEE journal of Quantum Electronics. QE-16, NO. **7**, 709 (1980).
[18] Nobuhiko Susa, Yoshiharu Yamauchi, Hiroaki Ando. IEEE Electron Device Letters. EDL-I, NO. **4**, 55 (1980).

*Corresponding author: yjz886666@yahoo.com.cn